Surface superconductivity emerged from disordered surface in undoped $BaFe_2As_2$

Quanxin Hu,[1,2] Fazhi Yang,[1,2] Xingyu Wang,[1,2] Jiajun Li,[1,2] Wenyao Liu,[3] Lingyuan Kong,[1,*] Shiliang Li,[1,2,5] Lei Yan,[1] Jinpeng Xu,[1,2,4,†] and Hong Ding[1,4,6,‡]

[1]*Beijing National Laboratory for Condensed Matter Physics and Institute of Physics, Chinese Academy of Sciences; Beijing 100190, China*

[2]*School of Physical Sciences, University of Chinese Academy of Sciences, Beijing 100190, China*

[3]*Laboratory for Assembly and Spectroscopy of Emergence, Boston College, Boston, 02467 Massachusetts, USA*

[4]*CAS Center for Excellence in Topological Quantum Computation, University of Chinese Academy of Sciences, Beijing 100190, China*

[5]*Songshan Lake Materials Laboratory, Dongguan, Guangdong 523808, China*

[6]*Tsung-Dao Lee Institute and School of Physics and Astronomy, Shanghai Jiao Tong University, Shanghai 200240, China*

(Received 22 November 2022; revised 15 February 2023; accepted 13 March 2023; published 29 March 2023)

Among the iron-based superconductors, "122"-type compounds have been widely studied due to the availability of high-quality single crystals. However, due to lack of a natural cleavage plane, the cleaved surface is usually polarized, which allows doping change or structure modification on the surface. In this paper, we propose a simple method to successfully transform the 122-type parent compound $BaFe_2As_2$ to a superconductor via room-temperature relaxation or uniaxial strain. Using scanning tunneling microscopy/spectroscopy, we demonstrate that this superconductivity results directly from the disordered surface morphologies. Based on the transport results and the disappearance of superconductivity with every new cleave, we conclude that the superconductivity only manifests at the most superficial surface. Our finding opens up an unexpected way to achieve superconductivity in undoped $BaFe_2As_2$, other than chemical doping, which may offer an alternative channel to understand the iron-based superconductivity and its connection with disorders.

DOI: 10.1103/PhysRevMaterials.7.034801

I. INTRODUCTION

Superconductivity is a well-explored phenomenon that has been observed in many materials upon cooling to very low temperatures. Conventional superconductivity has been readily described by the well-known Bardeen–Cooper–Schrieffer theory [1]. However, the discovery of unconventional superconductors challenges and extends this paradigm in an unexpected way [2]. In the case of iron-based superconductors (FeSCs), electron-electron interactions and multi-orbital characteristics give rise to a complicated phase diagram [3]. Hund's interaction is believed to play an important role in the normal state of FeSCs [4–12]. Besides the superconductivity, other electronic orders, such as magnetic order [13] and nematic order [14], emerge from the normal state before the system goes into a superconducting state.

The alkaline-earth iron pnictide $BaFe_2As_2$ (122 type) with $ThCr_2Si_2$ structure is one of the most investigated iron-based materials [15]. In the undoped form, $BaFe_2As_2$ is generally not superconducting under normal conditions with an orthorhombic antiferromagnetic ground state at low temperature [16]. Although it is well known that superconductivity can be achieved by applying pressure [17,18] or doping (isovalent doping, e.g., using P to substitute As; acceptor doping, e.g., using K to substitute Ba; donor doping, e.g., using Co to substitute Fe) [19,20], some undoped as-grown $BaFe_2As_2$ samples can exhibit traces of superconductivity with a superconducting transition temperature (T_c) around 20 K; e.g., the resistivity ρ of some samples shows a significant drop at 20 K as previously reported [21]. Similar results have also been observed in other 122-type iron pnictides [22]. The resistivity of $SrFe_2As_2$ actually goes to zero along with partial diamagnetic screening [23]. Strain or lattice distortion was thought to be the trigger for the superconductivity in these undoped 122-type iron pnictides. Meanwhile, Kim *et al.* disregarded strain as the cause for the superconductivity in their in-flux-grown $BaFe_2As_2$ and attributed it to the self-doping caused by crystal defects [24]. Adding to the puzzle, people also observed water-vapor-induced superconductivity around 20 K in $SrFe_2As_2$ thin films [25]. In addition, a 5–10 μm thick superconducting layer was observed on the surface of the nominal undoped $BaFe_2As_2$ after exposing to fluorine gas [26]. Interfacial superconductivity was found in 122-type parent compounds by simple subsequent annealing of the as-grown samples in an atmosphere of As, P, or Sb [27]. Different thermal history can induce the self-flux-grown $CaFe_2As_2$ to undergo different structural phase transitions

*Present address: T. J. Watson Laboratory of Applied Physics and Institute for Quantum Information and Matter, California Institute of Technology, Pasadena, CA 91125, USA.

†xujp@iphy.ac.cn

‡dingh@sjtu.edu.cn

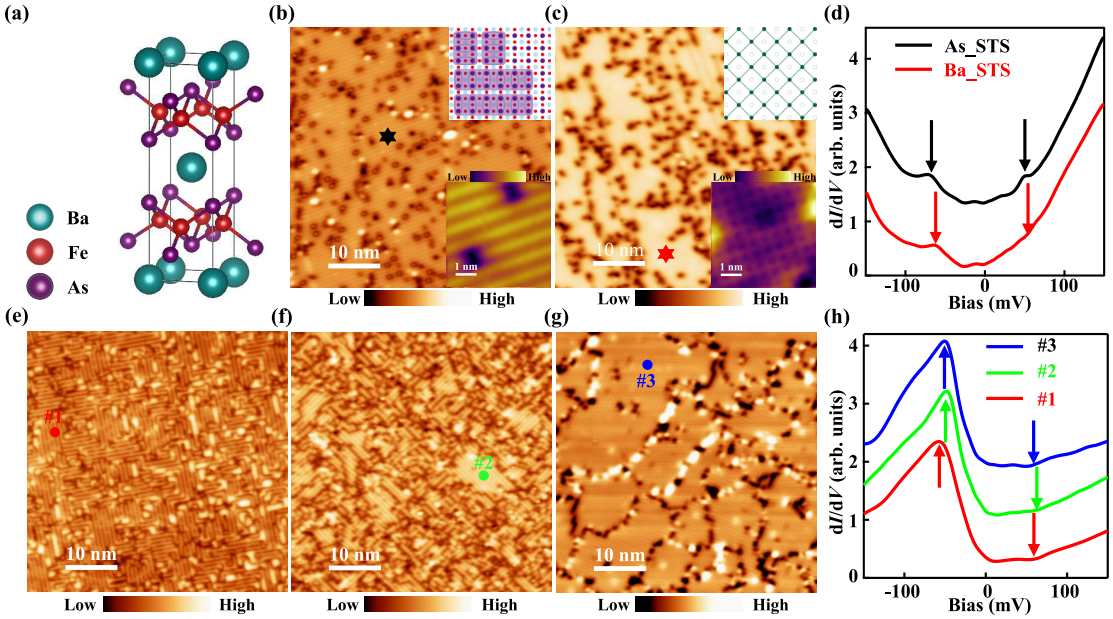

FIG. 1. STM topographic images and dI/dV spectra of $BaFe_2As_2$ cleaved at different temperatures. (a) Crystal structure of $BaFe_2As_2$. (b), (c) Summary of topographic images taken from various locations cleaved at 77 K ($U = 70$ mV, $I_t = 30$ pA). Upper insets in (b), (c) are schematic drawings for the 1×2 dimers and $(\sqrt{2} \times \sqrt{2})R45$ surface reconstructions (upper As: purple; lower As: light blue; Fe: red; Ba: green). Lower insets in (b), (c) are zoomed-in images for the 1×2 dimers and $(\sqrt{2} \times \sqrt{2})R45$ surface reconstructions [(b) $U = 70$ mV, $I_t = 200$ pA; (c) $U = -50$ mV, $I_t = 6$ nA). (d) Typical dI/dV spectra on 77 K–cleaved samples. The black dI/dV curve was taken on the As dimer surface and the red dI/dV curve was taken on the Ba surface. (e)–(g) Summary of topographic images taken from various locations cleaved at 300 K [(e), (f) $U = 500$ mV, $I_t = 100$ pA; (g) $U = 100$ mV, $I_t = 50$ pA]. (h) Typical dI/dV spectra on samples cleaved at 300 K.

at low temperature. Superconductivity was observed in the collapsed phase [28] and mixture phase [29,30]. By superlattice engineering, the bonding distance and As-Fe-As bond angle can be altered in a well-controlled way because of the lattice mismatch between the iron-based superconducting thin film and the substrate [31,32]. Superconductivity has been found in an undoped $BaFe_2As_2$ thin film grown on Fe-buffered $MgAl_2O_4$ [33] and in $BaFe_2As_2/SrTiO_3$ superlattice [34,35].

In order to apply advanced surface sensitive measurement techniques such as scanning tunneling microscopy/spectroscopy (STM/S), one needs to obtain a clean surface in vacuum while preserving the bulk stoichiometry and structure. The polar surface of a cleaved $BaFe_2As_2$ single crystal hinders intrinsic measurements of STM/S, in contrast to other FeSCs such as FeSe and LiFeAs, which have a clear and nonpolar surface that can minimize the surface effect [36,37]. As every coin has two sides, the polar surface can also give us a playground to explore interesting phenomena only existing on the surface which might shed light on the understanding of FeSCs. In this paper, we report a simple method to induce superconductivity on the surface of undoped parent compound $BaFe_2As_2$. Using STM/S we systematically studied the evolution of superconductivity on the surface of $BaFe_2As_2$. We found the emergence of superconductivity on the surface with room-temperature relaxation or applying uniaxial strain, accompanied by appearance of disorders of the ordered $BaFe_2As_2$ surface. We measured the superconducting gap (Δ_{sc}) and the superconducting transition temperature (T_c). Our results provide the hints of iron-based superconductivity and its relationship with disorders.

II. METHODS

Single crystals of $BaFe_2As_2$ were grown by the self-flux method. The flux FeAs was obtained by reacting the powder of Fe (99.99%) and As (99.99%) in an evacuated quartz tube at 740 °C. Then thin Ba (99+%) pieces and FeAs grains were mixed with a molar ratio of Ba:FeAs = 1:4 and the mixture was loaded into an Al_2O_3 crucible and sealed into a quartz tube. The tube was heated at 1180 °C for 10 h and slowly cooled to 1050 °C at a rate of 5 °C/h. The samples were cleaved in ultrahigh vacuum and inserted into the STM head immediately after cleaving. The STM measurement was carried out at 4.2 K unless otherwise described. STM/S measurements were carried out in ultralow-temperature STM with a 16 T magnet (Unisoku USM1300). The energy resolution is better than 0.19 meV with an effective electron temperature of 0.67 K. Tungsten tips made by electrochemical etching were used after electron beam heating and calibrated on a clean Au(111) surface.

III. RESULTS AND DISCUSSIONS

The crystal structure of the parent compound $BaFe_2As_2$ is shown in Fig. 1(a). The weakest bonding between the adjacent As and Ba layers is believed to be broken during a typical cleave process, which exposes two inequivalent surfaces formed by As or Ba atoms. As both Ba and As layers are polar surfaces, surface reconstruction may occur to equilibrate the

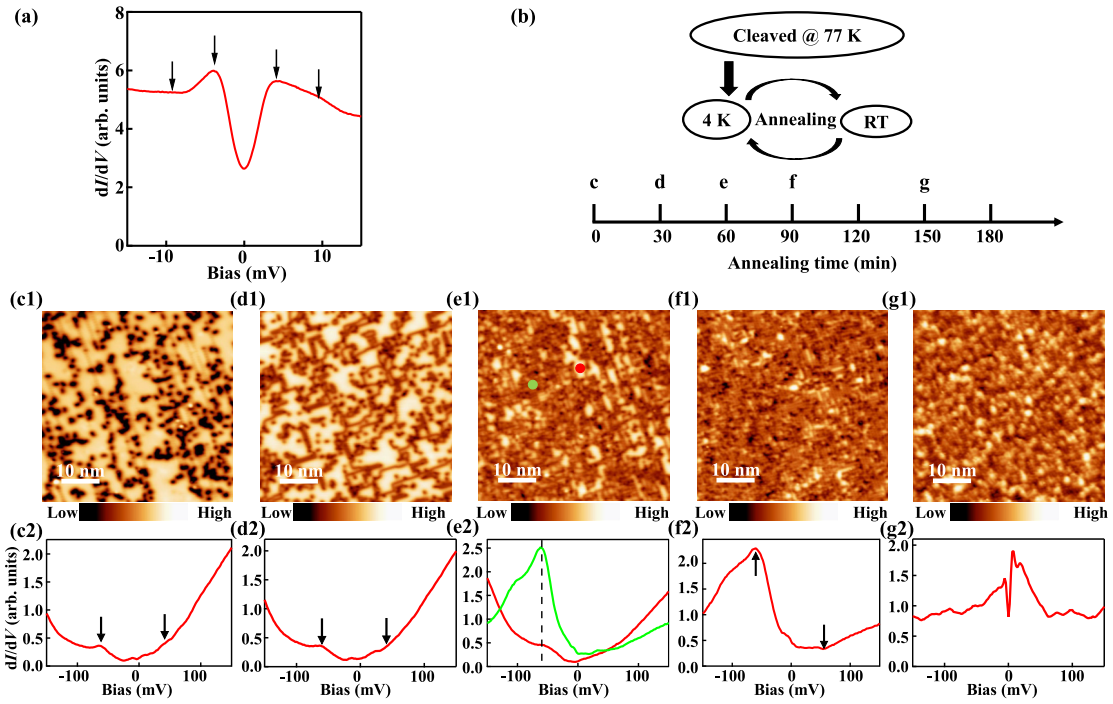

FIG. 2. Relaxation experiment for $BaFe_2As_2$. (a) dI/dV spectra were measured after the room-temperature relaxation process. The gap shows a multigap feature indicated by the black arrows. (b) Schematic diagram for relaxation process. The number on the axis represents the relaxation time. Topographic images after each circle are shown in (c)–(g). (c1,c2) Constant-current image for $BaFe_2As_2$ cleaved at 77 K ($U = 70$ mV, $I_t = 30$ pA) and corresponding spectra taken on the Ba termination ($U = 100$ mV, $I_t = 200$ pA). (d1–g1) Constant-current image after different relaxation time labeled in (b) ($U = 100$ mV, $I_t = 30$ pA). (d2–g2) Corresponding dI/dV spectra taken at the region (d1–g1) after the specific relaxation time ($U = 100$ mV; $I_t = 200$ pA).

unbalanced charge distribution [38–43]. As a result, various morphologies or terminations on the cleaved surface could make the properties of the surface distinct from the bulk materials. After extensive experiments on different samples cleaved at room temperature and 77 K without any relaxation process, we summarize the typical images in Fig. 1. Based on previous STM studies, two major surface reconstructions cleaved at 77 K can be assigned for the surface termination [41]: (1) As shown in the upper insets in Fig. 1(b), almost all the Ba atoms are removed, and the few remaining Ba atoms form scattered clusters instead of a complete atomic layer. The exposed As layer is reconstructed with the 1×2 superstructure. Lower insets in Fig. 1(b) show the 1×2 superstructure consisting of one-dimensional stripes with interstripe distance ~7.9 Å. (2) As shown in the upper insets in Fig. 1(c), many more Ba atoms are left on the lower As layer; they are equally distributed on the adjacent As surfaces and form a $(\sqrt{2} \times \sqrt{2})R45$ reconstruction. The lattice constant of 5.7 Å appears clearly in the lower insets in Fig. 1(c). Figure 1(c) shows the flat Ba termination with some vacancies. Figure 1(d) depicts a typical dI/dV spectrum taken on the flat area cleaved at 77 K with no adatoms or defects, which is consistent with previous work [42]. The spectra taken on different terminations share the same shape with some noticeable density of states (DOS) features indicated by the black and red arrows in Fig. 1(d). The DOS features on the two terminations have a small energy shift, which may indicate different chemical potentials. However, when cleaved at room temperature, the surface morphology becomes more complex [43]. Figure 1(e) shows a mazelike surface constituted by a 1×2 As dimer after being cleaved at room temperature. Figures 1(f) and 1(g) show short and long 1×2 ordered As-dimer stripes, respectively. The bright spots in the random distribution on the surface are the Ba atoms. Figure 1(h) displays several spectra taken on different surfaces cleaved at room temperature. Compared to the spectrum taken on the surface cleaved at 77 K, the spectra have a much stronger DOS peak at negative bias. We must emphasize that even though the dI/dV spectra are different under different cleavage conditions, the spectra on different locations under the same cleavage condition are almost the same except for the small shift of the peaks of DOS. The low density of states near the Fermi level indicates that undoped $BaFe_2As_2$ is a poor metal without superconductivity at 4.2 K.

A useful technique to modify the morphologies is room-temperature relaxation in an ultrahigh vacuum chamber, since the unstable polar surface can be easily influenced by external perturbations. Remarkably, we obtained superconductivity in all the relaxed samples cleaved at 77 K (superconductivity is also obtained on a relaxed sample cleaved at room temperature as shown in Fig. 6 in Appendix A). A typical observed superconducting spectrum is shown in Fig. 2(a), which indicates a multigap superconductivity, and the values of the two gaps are similar as the reported bulk superconducting

gaps of the superconducting $Ba_{0.6}K_{0.4}Fe_2As_2$ [44,45]. We systematically studied the evolution of this superconductivity. We did the room-temperature relaxation process following the schematic shown in Fig. 2(b). The sample was cleaved at 77 K in ultrahigh vacuum ($< 2 \times 10^{-10}$ Torr) and immediately inserted into the STM head, which was already at the base temperature (~4.2 K). After the measurement, we transferred the sample out of the STM head and relaxed it at room temperature in an ultrahigh vacuum environment. Then the sample was inserted back into the STM head and measured again. This relaxation measurement cycle can be repeated several times as shown in Fig. 2(b). Figure 2(c1) shows the most commonly observed morphology for the pristine surface with a $(\sqrt{2} \times \sqrt{2})R45$ reconstruction with the half Ba coverage. Although there are inevitable Ba vacancies on the surface, Ba atoms cover the termination almost completely. We first measured spectra on the Ba termination at 4.2 K. Similar to the earlier STM results, the tunneling spectrum preserves the same shape with arresting DOS features at −62 and 42 mV as indicated by the black arrows in Fig. 2(c2). After 30 min of room-temperature relaxation, the coverage of Ba atoms decreases. Small patches of the Ba atomic layer appear first, as shown in Fig. 2(d1). The tunneling spectrum taken on the flat area without adatoms and defects has the same shape as the spectrum taken on the pristine surface in Fig. 2(c2). With increasing the relaxation time, the coverage of Ba atoms declines further. At the same time, a disordered stripe structure appears, as shown in Fig. 2(e1). Spectra taken on the flat area (the red dot) and the disordered stripe region (the green dot) have different characteristics. Compared to the spectrum measured at the red dot, the spectrum taken at the green dot has a much stronger peak at −62 mV, as shown in Fig. 2(e2), which is similar to the spectrum taken on the surface cleaved at room temperature. After 90 min of room-temperature relaxation, as displayed in Fig. 2(f1), the majority of terminations form the disordered stripe structure, and the spectrum restores to the dI/dV curves measured on samples cleaved at room temperature, as shown in Fig. 2(f2). After 150 min relaxation, the surface morphology becomes more disorganized with very short stripes and bright adatoms randomly distributed as shown in Fig. 2(g1). Most strikingly, the tunneling spectrum shows that the density of states increase around the Fermi level, and a dip precisely located at 0 mV is visible in Fig. 2(g2). Further experiment confirms that this dip is a superconducting gap.

In addition to relaxation at room temperature, a uniaxial strain is another method for modifying the surface. Thus, we carried out STM/S measurements on $BaFe_2As_2$ cleaved at room temperature under the uniaxial strain applied by a homemade device [46]. With this simple device, a strain along a specific direction can be applied on the sample. Whether we apply the stress in the [110] or [100] direction, whether we cleave first and then apply the uniaxial stress, or vice versa, we always end up with the surface morphology depicted in Figs. 3(a)–3(c). There is no ordered surface reconstruction in this case, similar to the case of room-temperature relaxation. Long-range order is lost on the surface. Figure 3(d) displays the averaged dI/dV spectra from specific surfaces. The blue curve is taken from the room-temperature cleaved surface without strain. The dI/dV spectra obtained on the surface of the strained sample concur with what we observed in Fig. 2(g2) for the relaxed sample without strain, with a clear dip precisely located at 0 mV. In both the relaxed and strained samples, a disordered surface is invariably accompanied by superconductivity.

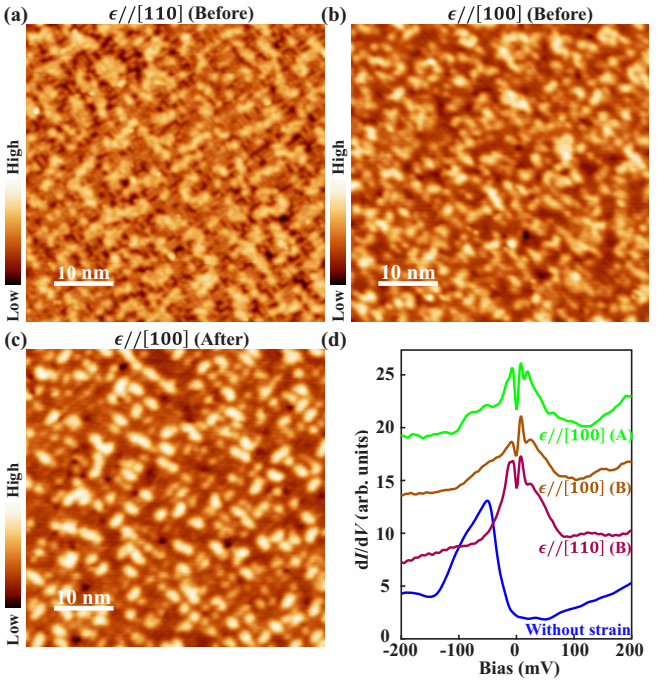

FIG. 3. Uniaxial strained $BaFe_2As_2$ cleaved at room temperature. (a) Typical STM topography for $BaFe_2As_2$ strained along the [110] direction ($U = 100$ mV, $I_t = 50$ pA). After applying uniaxial stress, the sample was cleaved at room temperature. (b) Typical STM topography for $BaFe_2As_2$ strained along the [100] direction ($U = 100$ mV, $I_t = 30$ pA). The sample was cleaved at room temperature after applying uniaxial stress. (c) Typical STM topography for $BaFe_2As_2$ strained along the [100] direction ($U = 100$ mV, $I_t = 30$ pA). The sample was cleaved at room temperature and then uniaxial stress was applied. (d) Averaged dI/dV spectra from specific surfaces. The spectra from the room-temperature cleaved surface without uniaxial stress is also plotted for comparison. The spectra are shifted for clarity.

To verify the nature of superconductivity for this observed gap, we conducted more detailed measurements on the sample relaxed for 150 min, as shown in Fig. 4 (the superconducting gap taken on the uniaxial strained sample is shown in Fig. 7 in Appendix B). The surface topographic image is shown in Fig. 4(a). Figure 4(b) shows the spectra recorded along the black line in Fig. 4(a). The vertical dashed lines in the figure indicate the average positions of the symmetric coherence peaks, which demonstrates that the disordered surface exhibits an inhomogeneous superconducting gap. Here we use the distance between the two coherent peaks as the superconducting gap size $2\Delta_{sc}$. Figure 4(c) shows the histogram of the superconducting gap magnitude. Fitting the data using a Gaussian function, we get the mean gap value $\Delta_{sc} = 4.15$ meV and the standard deviation $\sigma = 0.58$ meV. The gap size observed here is qualitatively consistent with the

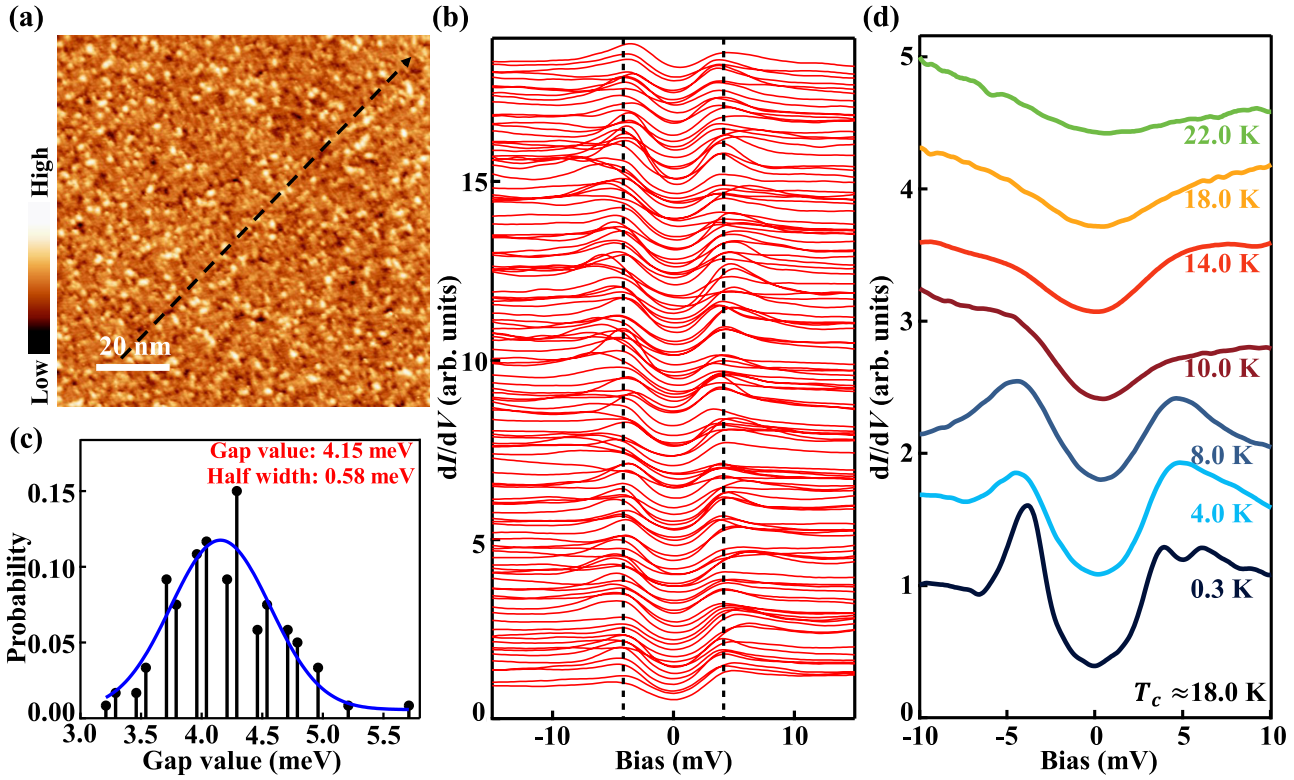

FIG. 4. (a) Topographic image of a disordered surface after 150 min relaxation ($U = 70$ mV, $I_t = 30$ pA). (b) Spatially resolved spectra taken along the arrow line in (a). Spectra are offset for clarity. All spectra were taken at 4.2 K. The two vertical dashed lines are a guide for the eyes. (c) Histogram of superconducting gap size obtained along the arrow line in (a). The blue curve is a fitting using Gaussian function. The mean gap value is 4.15 meV and the half width is 0.58 meV. (d) Temperature evolution of the superconducting gap. The spectra are shifted for clarity.

gap observed in electron-doped $Ba(Fe_{1-x}Co_x)_2As_2$ [47] and hole-doped $Ba_{1-x}K_xFe_2As_2$ [44,45]. As shown in Fig. 4(d), this gap is gradually suppressed at elevated temperatures and, eventually, the coherence peak disappears at $T_c \approx 18$ K. The corresponding gap ratio of $2\Delta_{sc}/k_BT_c \approx 5.34$ is larger than the predicted value of 3.53 in conventional BCS superconductors. The surface superconductivity that emerged after relaxation is further investigated by imaging magnetic vortices at 0.3 K as shown in Fig. 8 in Appendix C. Figure 8 shows a series of spectra measured along the white arrow line in Fig. 8(c). Upon approaching the vortex core, the superconducting gap is gradually suppressed, accompanied by vortex core states peaking at negative bias. We have also measured spectra at zero field at 0.3 K along the same trajectory as shown in Fig. 8(f). No additional in-gap features can be seen, which indicates that the observed vortex bound state is an intrinsic phenomenon instead of impurity states. Compared to the asymmetric vortex bound states observed in other iron-based superconductors, the bound states observed here are broader, which suggests that stronger scattering caused by the surface disorder smears out the bound states.

Despite the disordered surface after relaxation, a few areas of patches still exist that can identified with atomic resolution, such as As vacancy (red dot), Ba disorder (green dot), and 1×2 superstructure consisting of As dimer (blue dot), shown in Fig. 5(a). Figure 5(b) is a zero-bias conductance map taken in the same region as Fig. 5(a). In general, the zero-bias conductance is higher in the Ba disordered region. To demonstrate more clearly, the typical spectra taken from 1×2 superstructure, As vacancy, and Ba disorder at 0.3 K are shown in Fig. 5(c). The spectra are homogeneous within the 1×2 superstructure. The superconducting spectrum on the Ba disorder (green) shows a suppressed coherence peak and a shallower gap depth [defined by $1 - N(0)$, where $N(0)$ is the normalized dI/dV value at $V = 0$ mV], indicating a large impurity scattering effect. The common feature of these spectra is the existence of residual DOS inside the superconducting gap, which is different from $Ba_{0.6}K_{0.4}Fe_2As_2$ with negligible zero-bias conductance in the bright region [44]. Considering that there is no superconducting signal in transport measurement (Fig. 9 in Appendix D) and the sample is restored to "poor metal" after recleavage (Fig. 10 in Appendix E), we infer that only the top surface layers become superconducting after room-temperature relaxation. The residual DOS may come from the unpaired electrons below the surface or from the disorder-induced in-gap states.

We operated the same relaxation process for the samples cleaved at room temperature. In contrast to the surface cleaved at 77 K, the surface cleaved at room temperature has essentially no Ba atoms left on it. However, following relaxation, the surface becomes chaotic and also exhibits superconductivity. Additionally, uniaxial strain will not affect the surface

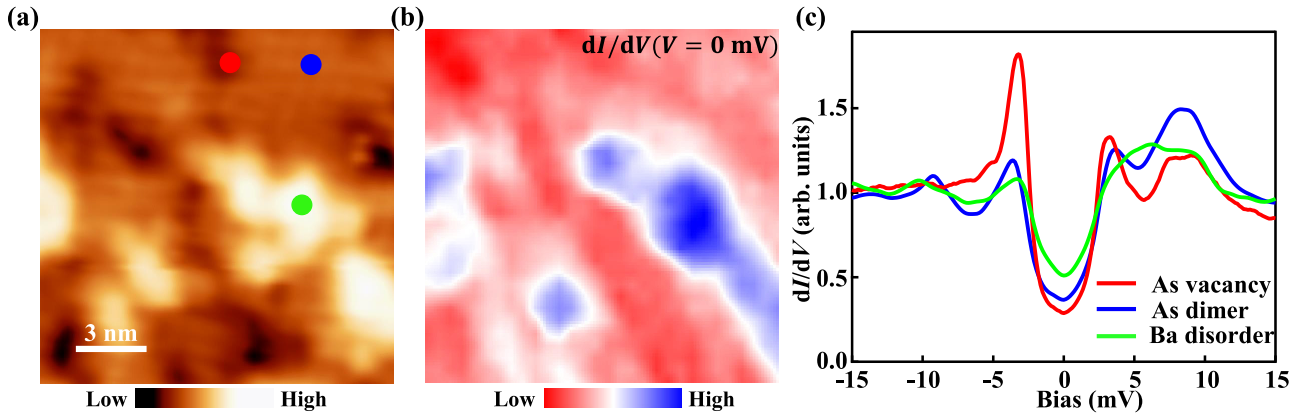

FIG. 5. (a), (b) Zoomed-in topographic image of a region with As dimer, As vacancy, and Ba disorder ($U = 30$ mV, $I_t = 30$ pA) and a dI/dV map taken at 0 mV for the same region. (c) Tunneling spectra taken at As dimer, As vacancy, and Ba disorder ($U = 15$ mV, $I_t = 200$ pA). All spectra were taken at 0.3 K.

doping. Inferring from these, we conclude that self-doping effects caused by Ba atoms escaping might not be the root of the surface superconductivity. In fact, the exposed surface of $BaFe_2As_2$ after cleavage might be away from the energetically stable surface. The observed topography in Fig. 1 is in a metastable state. Room-temperature relaxation and uniaxial strain can cause the surface atoms to be redistributed and relieve the surface lattice strain to minimize the surface energy. Thus, the surface becomes disordered, and the long-range order is disrupted. In the meantime, the peak of DOS at the negative bias moves to the Fermi level, which is beneficial to the formation of superconductivity. This shows that the disordered surface changes the electronic structure dramatically. In general, in the presence of severe disorder, superconductivity should be destroyed and possibly undergo a superconductor-insulator transition. The unusual surface superconductivity observed here possibly arises from the suppression of antiferromagnetic competing orders or multifractality of electron wave functions [48–50]. The disordered surface morphology and the relaxation of the surface lattice structure could be the favorable factors for the emergence of surface superconductivity in $BaFe_2As_2$. However, we admit that other possibilities in our system cannot be completely ruled out.

IV. CONCLUSION

In summary, we comprehensively studied the surface superconductivity of the parent compound $BaFe_2As_2$ induced by room-temperature relaxation and uniaxial strain. By using STM/S measurement, we determined the superconducting gap size and transition temperature. Because the superconductivity can be destroyed by recleaving the sample and because there is no superconducting signal in transport measurement, the superconductivity likely exists only on the surface. The origin of surface superconductivity is yet to be identified. Our observation reveals a simple way to achieve superconductivity in undoped $BaFe_2As_2$ by using the unstable polar surface. This unusual surface superconductivity offers valuable insights into the occurrence of superconductivity in the 122-type compounds.

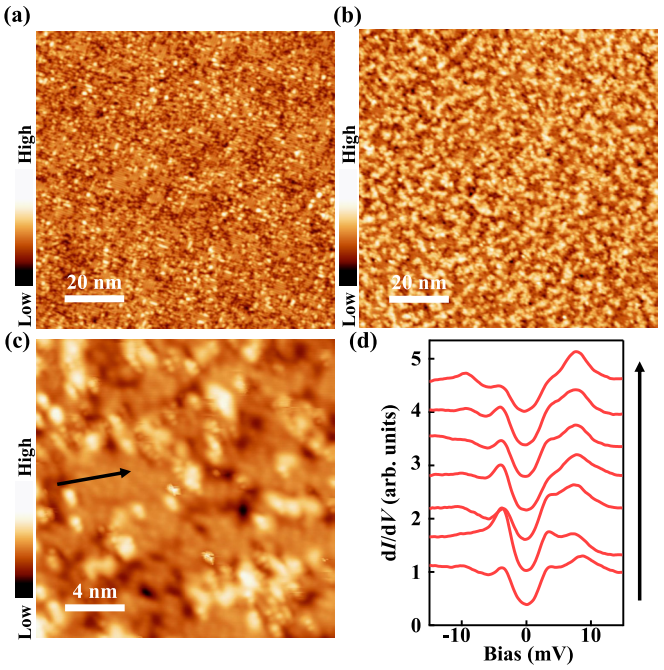

FIG. 6. (a) Constant-current STM topography taken on $BaFe_2As_2$ cleaved at room temperature without strain ($U = 600$ mV, $I_t = 100$ pA). (b) Constant-current STM topography taken on $BaFe_2As_2$ after room-temperature relaxation ($U = 500$ mV, $I_t = 100$ pA). (c) Enlarged constant-current STM topography taken on $BaFe_2As_2$ cleaved at room temperature after relaxation ($U = 60$ mV, $I_t = 100$ pA). (d) Spatially resolved spectra of dI/dV recorded along the trajectory (black line) indicated in (c). The spectra were taken at 0.3 K.

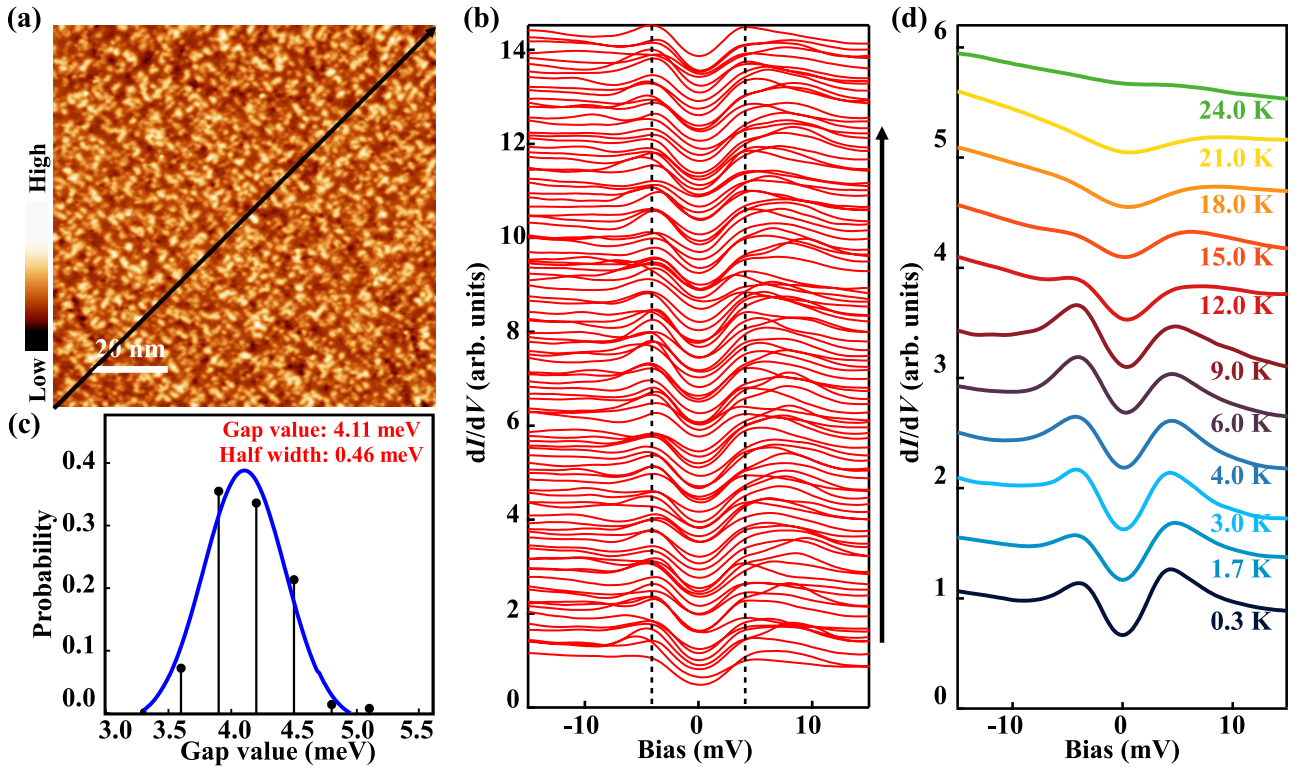

FIG. 7. (a) Topographic image of a disordered surface cleaved at room temperature with [100] direction strain ($U = 100$ mV, $I_t = 100$ pA). (b) Spatially resolved spectra taken along the black arrow line in (a). Spectra are offset for clarity. All spectra are taken at 4.2 K. (c) Histogram of superconducting gap size obtained along the arrow line in (b). The blue curve is a fitting using Gaussian function. The mean gap value is 4.11 meV and the half width is 0.46 meV. (d) Temperature evolution of the superconducting gap.

ACKNOWLEDGMENTS

The work at IOP is supported by grants from the National Natural Science Foundation of China (Grants No. 2019000043, No. 111920101005, No. 11888101, No. 11234014, No. 61888102, No. 11920101005, and No. 11921004), the Ministry of Science and Technology of China (Grants No. 2021ZD0302700, No. 2016YFA0202300, No. 2018YFA0305700, No. 2017YFA0302900, and No. 2019YFA0308500), and the Chinese Academy of Sciences (Grants No. BR201902, No. 2020000053, No. XDB28000000, No. XDB07000000, and No. 112111KYSB20160061). This work is partially supported by the Synergic Extreme Condition User Facility, Beijing, China.

Q.H., F.Y., and X.W. contributed equally to this work.

APPENDIX A

Unstrained $BaFe_2As_2$ was cleaved at room temperature, and a relaxation experiment was conducted. See Fig. 6.

APPENDIX B

A superconducting gap was taken on a uniaxial strained $BaFe_2As_2$ sample. See Fig. 7.

APPENDIX C

As Fig. 8 shows, the vortex and vortex bound state were observed in $BaFe_2As_2$ at 0.3 K.

APPENDIX D

See Fig. 9, which shows transport measurement for a uniaxial strained sample.

APPENDIX E

Figure 10 shows the 1st cleave - relaxation - 2nd re-cleave process.

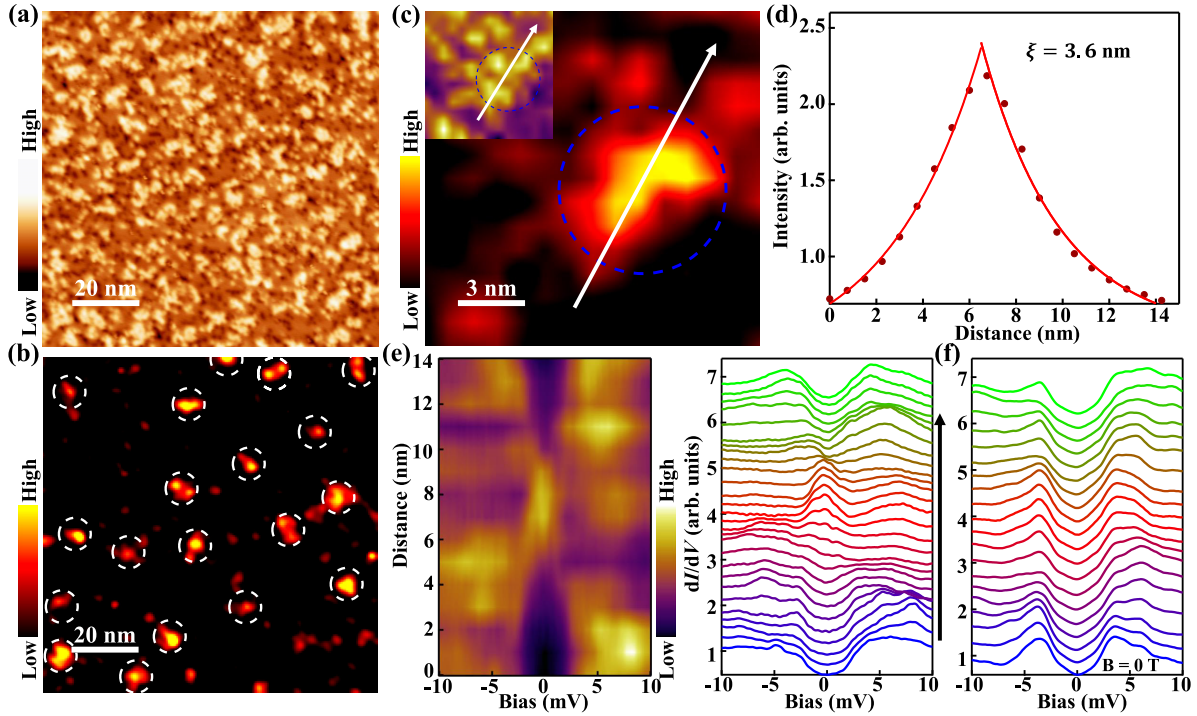

FIG. 8. (a), (b) Topographic image of a disordered surface after relaxation ($U = 70$ mV, $I_t = 30$ pA) and corresponding zero-bias conductance map at a magnetic field of 5 T. (c) A zero-bias conductance map around a vortex (area: 15 nm × 15 nm) taken at $T = 0.3$ K, $B = 5$ T. The inset is the topographic image of the vortex shown in (c). (d) Red solid circles are the line profile of the zero-bias conductance map of a vortex. The red line is the fitting result using the exponential decay function. The coherence length for the surface superconductivity is $\xi = 3.6$ nm. (e) Intensity plot of dI/dV and waterfall-like dI/dV spectra along the white arrow line across the vortex in (c). Spectra are offset for clarity. The black arrow represents the direction of the waterfall plot. (f) A series of spectra measured at 0 T along the same trajectory as that in (e).

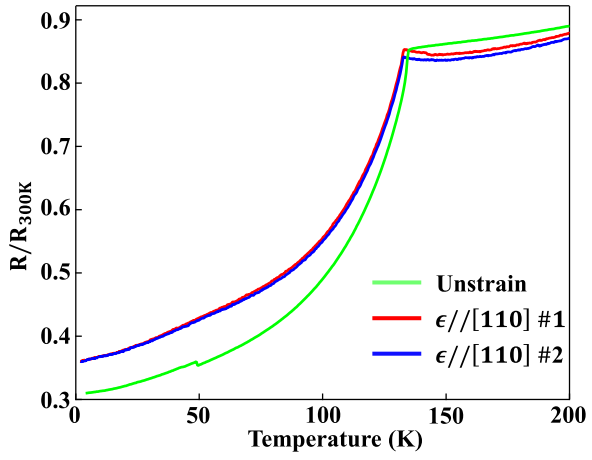

FIG. 9. Temperature-dependent resistivity with different strain. The measurements were carried out by a standard four-probe method. The green curve was taken on unstrained $BaFe_2As_2$. Red and blue curves were taken on the other sample with [110] direction strain.

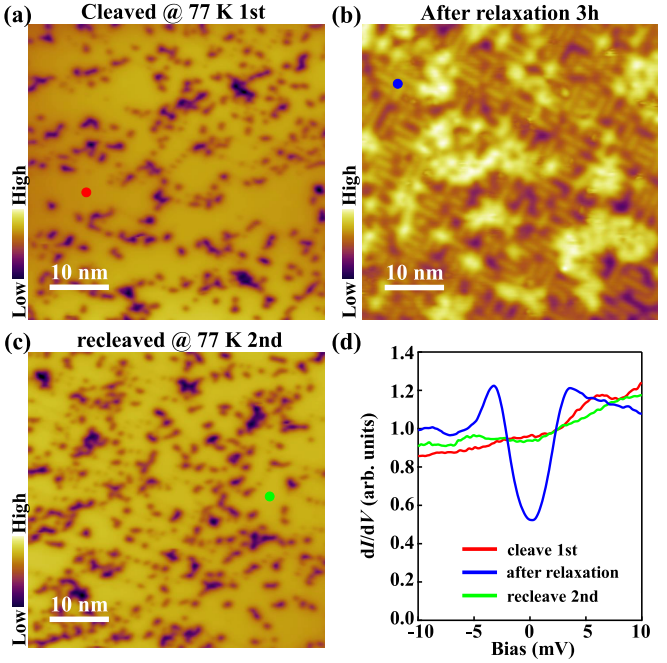

FIG. 10. (a) Topographic image of Ba surfaces cleaved at 77 K. (b) Topographic image of disordered surface after room-temperature relaxation. (c) Topographic image of $BaFe_2As_2$ after recleaving at 77 K ($U = 1$ V, $I_t = 100$ pA). (d) Corresponding dI/dV spectra taken at the region in (a)–(c) ($U = 10$ mV, $I_t = 200$ pA).

[1] J. Bardeen, L. N. Cooper, and J. R. Schrieffer, Theory of superconductivity, Phys. Rev. **108**, 1175 (1957).

[2] D. J. Scalapino, A common thread: The pairing interaction for unconventional superconductors, Rev. Mod. Phys. **84**, 1383 (2012).

[3] R. M. Fernandes, A. I. Coldea, H. Ding, I. R. Fisher, P. J. Hirschfeld, and G. Kotliar, Iron pnictides and chalcogenides: A new paradigm for superconductivity, Nature (London) **601**, 35 (2022).

[4] P. Werner, E. Gull, M. Troyer, and A. J. Millis, Spin Freezing Transition and Non-Fermi-Liquid Self-Energy in a Three-Orbital Model, Phys. Rev. Lett. **101**, 166405 (2008).

[5] K. Haule and G. Kotliar, Coherence–incoherence crossover in the normal state of iron oxypnictides and importance of Hund's rule coupling, New J. Phys. **11**, 025021 (2009).

[6] Z. P. Yin, K. Haule, and G. Kotliar, Kinetic frustration and the nature of the magnetic and paramagnetic states in iron pnictides and iron chalcogenides, Nat. Mater **10**, 932 (2011).

[7] Z. P. Yin, K. Haule, and G. Kotliar, Magnetism and charge dynamics in iron pnictides, Nat. Phys. **7**, 294 (2011).

[8] A. Georges, L. de' Medici, and J. Mravlje, Strong correlations from Hund's coupling, Annu. Rev. Condens. Matter Phys. **4**, 137 (2013).

[9] L. de' Medici, G. Giovannetti, and M. Capone, Selective Mott Physics as a Key to Iron Superconductors, Phys. Rev. Lett. **112**, 177001 (2014).

[10] K. M. Stadler, Z. P. Yin, J. von Delft, G. Kotliar, and A. Weichselbaum, Dynamical Mean-Field Theory Plus Numerical Renormalization-Group Study of Spin-Orbital Separation in a Three-Band Hund Metal, Phys. Rev. Lett. **115**, 136401 (2015).

[11] T.-H. Lee, A. Chubukov, H. Miao, and G. Kotliar, Pairing Mechanism in Hund's Metal Superconductors and the Universality of the Superconducting Gap to Critical Temperature Ratio, Phys. Rev. Lett. **121**, 187003 (2018).

[12] E. Walter, K. M. Stadler, S.-S. B. Lee, Y. Wang, G. Kotliar, A. Weichselbaum, and J. von Delft, Uncovering Non-Fermi-Liquid Behavior in Hund Metals: Conformal Field Theory Analysis of an Su (2) × Su (3) Spin-Orbital Kondo Model, Phys. Rev. X **10**, 031052 (2020).

[13] P. Dai, Antiferromagnetic order and spin dynamics in iron-based superconductors, Rev. Mod. Phys. **87**, 855 (2015).

[14] R. M. Fernandes, A. V. Chubukov, and J. Schmalian, What drives nematic order in iron-based superconductors? Nat. Phys. **10**, 97 (2014).

[15] D. Mandrus, A. S. Sefat, M. A. McGuire, and B. C. Sales, Materials chemistry of $BaFe_2As_2$: A model platform for unconventional superconductivity, Chem. Mater. **22**, 715 (2010).

[16] M. Rotter, M. Tegel, D. Johrendt, I. Schellenberg, W. Hermes, and R. Pöttgen, Spin-density-wave anomaly at 140 K in the ternary iron arsenide $BaFe_2As_2$, Phys. Rev. B **78**, 020503(R) (2008).

[17] P. L. Alireza, Y. T. C. Ko, J. Gillett, C. M. Petrone, J. M. Cole, G. G. Lonzarich, and S. E. Sebastian, Superconductivity up to 29 K in $SrFe_2As_2$ and $BaFe_2As_2$ at high pressures, J. Phys.: Condens. Matter **21**, 012208 (2008).

[18] T. Yamazaki, N. Takeshita, R. Kobayashi, H. Fukazawa, Y. Kohori, K. Kihou, C.-H. Lee, H. Kito, A. Iyo, and H. Eisaki, Appearance of pressure-induced superconductivity in $BaFe_2As_2$ under hydrostatic conditions and its extremely high sensitivity to uniaxial stress, Phys. Rev. B **81**, 224511 (2010).

[19] S. Ishida, D. Song, H. Ogino, A. Iyo, H. Eisaki, M. Nakajima, J.-i. Shimoyama, and M. Eisterer, Doping-dependent critical current properties in K, Co, and P-doped $BaFe_2As_2$ single crystals, Phys. Rev. B **95**, 014517 (2017).

[20] P. C. Canfield and S. L. Bud'ko, FeAs-based superconductivity: A case study of the effects of transition metal doping on $BaFe_2As_2$, Annu. Rev. Condens. Matter Phys. **1**, 27 (2010).

[21] M. A. Tanatar, N. Ni, G. D. Samolyuk, S. L. Bud'ko, P. C. Canfield, and R. Prozorov, Resistivity anisotropy of AFe_2As_2 (A = Ca Sr, Ba): Direct versus Montgomery technique measurements, Phys. Rev. B **79**, 134528 (2009).

[22] M. S. Torikachvili, S. L. Bud'ko, N. Ni, P. C. Canfield, and S. T. Hannahs, Effect of pressure on transport and magnetotransport properties in $CaFe_2As_2$ single crystals, Phys. Rev. B **80**, 014521 (2009).

[23] S. R. Saha, N. P. Butch, K. Kirshenbaum, J. Paglione, and P. Y. Zavalij, Superconducting and Ferromagnetic Phases Induced by Lattice Distortions in Stoichiometric $SrFe_2As_2$ Single Crystals, Phys. Rev. Lett. **103**, 037005 (2009).

[24] J. S. Kim, T. D. Blasius, E. G. Kim, and G. R. Stewart, Superconductivity in undoped single crystals of $BaFe_2As_2$: Field and current dependence, J. Phys.: Condens. Matter **21**, 342201 (2009).

[25] H. Hiramatsu, T. Katase, T. Kamiya, M. Hirano, and H. Hosono, Water-induced superconductivity in $SrFe_2As_2$, Phys. Rev. B **80**, 052501 (2009).

[26] G. N. Tam, H. Maruyama, J. C. Nino, and G. R. Stewart, 22 K superconductivity in $BaFe_2As_2$ exposed to F_2, Phys. Rev. B **102**, 134507 (2020).

[27] S. Huyan, Y. Lyu, H. Wang, L. Deng, Z. Wu, B. Lv, K. Zhao, F. Tian, G. Gao, R. Liu *et al.*, Interfacial superconductivity achieved in parent $AEFe_2As_2$ (AE = Ca, Sr, Ba) by a simple and realistic annealing route, Nano Lett. **21**, 2191 (2021).

[28] D.-Y. Chen, J. Yu, B.-B. Ruan, Q. Guo, L. Zhang, Q.-G. Mu, X.-C. Wang, B.-J. Pan, G.-F. Chen, and Z.-A. Ren, Superconductivity in undoped $CaFe_2As_2$ single crystals, Chin. Phys. Lett. **33**, 067402 (2016).

[29] K. Zhao, B. Lv, L. Deng, S.-Y. Huyan, Y.-Y. Xue, and C.-W. Chu, Interface-induced superconductivity at ∼25 K at ambient pressure in undoped $CaFe_2As_2$ single crystals, Proc. Natl. Acad. Sci. USA **113**, 12968 (2016).

[30] S. Huyan, L. Z. Deng, Z. Wu, K. Zhao, J. Y. Sun, L. J. Wu, Y. Y. Zhao, H. M. Yuan, M. Gooch, B. Lv *et al.*, Low-temperature microstructural studies on superconducting $CaFe_2As_2$, Sci. Rep. **9**, 6393 (2019).

[31] H. Sato, H. Hiramatsu, T. Kamiya, and H. Hosono, Strain engineering at heterointerfaces: Application to an iron pnictide superconductor, cobalt-doped $BaFe_2As_2$, ACS Appl. Mater. Interfaces **12**, 50096 (2020).

[32] J.-H. Kang, L. Xie, Y. Wang, H. Lee, N. Campbell, J. Jiang, P. J. Ryan, D. J. Keavney, J.-W. Lee, T. H. Kim *et al.*, Control of epitaxial $BaFe_2As_2$ atomic configurations with substrate surface terminations, Nano Lett. **18**, 6347 (2018).

[33] J. Engelmann, V. Grinenko, P. Chekhonin, W. Skrotzki, D. V. Efremov, S. Oswald, K. Iida, R. Hühne, J. Hänisch, M. Hoffmann *et al.*, Strain induced superconductivity in the parent compound $BaFe_2As_2$, Nat. Commun. **4**, 2877 (2013).

[34] J.-H. Kang, J.-W. Kim, P. J. Ryan, L. Xie, L. Guo, C. Sundahl, J. Schad, N. Campbell, Y. G. Collantes, E. E. Hellstrom *et al.*, Superconductivity in undoped $BaFe_2As_2$ by tetrahedral geometry design, Proc. Natl. Acad. Sci. USA **117**, 21170 (2020).

[35] J.-H. Kang, P. J. Ryan, J.-W. Kim, J. Schad, J. P. Podkaminer, N. Campbell, J. Suttle, T. H. Kim, L. Luo, D. Cheng *et al.*, Local atomic configuration control of superconductivity in the undoped pnictide parent compound $BaFe_2As_2$, ACS Appl. Electron. Mater. **4**, 1511 (2022).

[36] P. Richard, T. Sato, K. Nakayama, T. Takahashi, and H. Ding, Fe-based superconductors: An angle-resolved photoemission spectroscopy perspective, Rep. Prog. Phys. **74**, 124512 (2011).

[37] J. E. Hoffman, Spectroscopic scanning tunneling microscopy insights into Fe-based superconductors, Rep. Prog. Phys. **74**, 124513 (2011).

[38] F. Massee, Y. Huang, R. Huisman, S. de Jong, J. B. Goedkoop, and M. S. Golden, Nanoscale superconducting-gap variations and lack of phase separation in optimally doped $BaFe_{1.86}Co_{0.14}As_2$, Phys. Rev. B **79**, 220517(R) (2009).

[39] Y. Yin, M. Zech, T. L. Williams, X. F. Wang, G. Wu, X. H. Chen, and J. E. Hoffman, Scanning Tunneling Spectroscopy and Vortex Imaging in the Iron Pnictide Superconductor $BaFe_{1.8}Co_{0.2}As_2$, Phys. Rev. Lett. **102**, 097002 (2009).

[40] H. Zhang, J. Dai, Y. Zhang, D. Qu, H. Ji, G. Wu, X. F. Wang, X. H. Chen, B. Wang, C. Zeng *et al.*, $\sqrt{2} \times \sqrt{2}$ Structure and charge inhomogeneity at the surface of superconducting $BaFe_{2-x}Co_xAs_2 (x = 0 - 0.32)$, Phys. Rev. B **81**, 104520 (2010).

[41] A. Li, J.-X. Yin, J. Wang, Z. Wu, J. Ma, A. S. Sefat, B. C. Sales, D. G. Mandrus, M. A. McGuire, R. Jin *et al.*, Surface terminations and layer-resolved tunneling spectroscopy of the 122 iron pnictide superconductors, Phys. Rev. B **99**, 134520 (2019).

[42] V. B. Nascimento, A. Li, D. R. Jayasundara, Y. Xuan, J. O'Neal, S. Pan, T. Y. Chien, B. Hu, X. B. He, G. Li *et al.*, Surface Geometric and Electronic Structures of $BaFe_2As_2(001)$, Phys. Rev. Lett. **103**, 076104 (2009).

[43] F. Massee, S. de Jong, Y. Huang, J. Kaas, E. van Heumen, J. B. Goedkoop, and M. S. Golden, Cleavage surfaces of the $BaFe_{2-x}Co_xAs_2$ and $Fe_ySe_{1-x}Te_x$ Superconductors: A combined STM plus LEED study, Phys. Rev. B **80**, 140507(R) (2009).

[44] L. Shan, Y.-L. Wang, B. Shen, B. Zeng, Y. Huang, A. Li, D. Wang, H. Yang, C. Ren, Q.-H. Wang *et al.*, Observation of ordered vortices with Andreev bound states in $Ba_{0.6}K_{0.4}Fe_2As_2$, Nat. Phys **7**, 325 (2011).

[45] L. Shan, Y.-L. Wang, J. Gong, B. Shen, Y. Huang, H. Yang, C. Ren, and H.-H. Wen, Evidence of multiple nodeless energy gaps in superconducting $Ba_{0.6}K_{0.4}Fe_2As_2$ single crystals from scanning tunneling spectroscopy, Phys. Rev. B **83**, 060510(R) (2011).

[46] W. Liu, Q. Hu, X. Wang, Y. Zhong, F. Yang, L. Kong, L. Cao, G. Li, K. Okazaki, T. Kondo *et al.*, Tunable vortex Majorana modes controlled by strain in homogeneous LiFeAs, Quantum Front **1**, 20 (2022).

[47] Q. Zou, Z. Wu, M. Fu, C. Zhang, S. Rajput, Y. Wu, L. Li, D. S. Parker, J. Kang, A. S. Sefat *et al.*, Effect of surface morphology and magnetic impurities on the electronic structure in cobalt-doped $BaFe_2As_2$ superconductors, Nano Lett. **17**, 1642 (2017).

[48] M. V. Feigel'man, L. B. Ioffe, V. E. Kravtsov, and E. A. Yuzbashyan, Eigenfunction Fractality and Pseudogap State near the Superconductor-Insulator Transition, Phys. Rev. Lett. **98**, 027001 (2007).

[49] K. Zhao, H. Lin, X. Xiao, W. Huang, W. Yao, M. Yan, Y. Xing, Q. Zhang, Z.-X. Li, S. Hoshino *et al.*, Disorder-induced multifractal superconductivity in monolayer niobium dichalcogenides, Nat. Phys. **15**, 904 (2019).

[50] I. S. Burmistrov, I. V. Gornyi, and A. D. Mirlin, Superconductor-insulator transitions: Phase diagram and magnetoresistance, Phys. Rev. B **92**, 014506 (2015).